LINEARLY IMPLICIT IMEX RUNGE-KUTTA METHODS FOR A CLASS OF DEGENERATE CONVECTION-DIFFUSION PROBLEMS

SEBASTIANO BOSCARINO*, RAIMUND BÜRGER†, PEP MULET‡, GIOVANNI RUSSO§, AND LUIS M. VILLADA¶

Abstract. Multi-species kinematic flow models with strongly degenerate diffusive corrections give rise to systems of nonlinear convection-diffusion equations of arbitrary size. Applications of these systems include models of polydisperse sedimentation and multi-class traffic flow. Implicit-explicit (IMEX) Runge-Kutta (RK) methods are suitable for the solution of these convection-diffusion problems since the stability restrictions, coming from the explicitly treated convective part, are much less severe than those that would be deduced from an explicit treatment of the diffusive term. These schemes usually combine an explicit Runge-Kutta scheme for the time integration of the convective part with a diagonally implicit one for the diffusive part. In [R. Bürger, P. Mulet and L.M. Villada, *SIAM J. Sci. Comput.*, 35 (2013), pp. B751–B777] a scheme of this type is proposed, where the nonlinear and non-smooth systems of algebraic equations arising in the implicit treatment of the degenerate diffusive part are solved by smoothing of the diffusion coefficients combined with a Newton-Raphson method with line search. This nonlinearly implicit method is robust but associated with considerable effort of implementation and possibly CPU time. To overcome these shortcomings while keeping the advantageous stability properties of IMEX-RK methods, a second variant of these methods is proposed, in which the diffusion terms are discretized in a way that more carefully distinguishes between stiff and nonstiff dependence, such that in each time step only a linear system needs to be solved still maintaining high order accuracy in time, which makes these methods much simpler to implement. In a series of examples of polydisperse sedimentation and multi-class traffic flow it is demonstrated that these new linearly implicit IMEX-RK schemes approximate the same solutions as the nonlinearly implicit versions, and in many cases these schemes are more efficient.

Key words. Implicit-explicit Runge-Kutta schemes, degenerate convection-diffusion equations, linearly implicit methods, polydisperse sedimentation, multiclass traffic flow.

1. Introduction.

1.1. Scope. This paper is concerned with numerical methods for systems of nonlinear convection-diffusion equations of the type

$$\partial_t \Phi + \partial_x \boldsymbol{f}(\Phi) = \partial_x \big(\boldsymbol{B}(\Phi) \partial_x \Phi \big), \tag{1.1}$$

where $\Phi = (\phi_1, \ldots, \phi_N)^{\mathrm{T}}$ is the sought solution as a function of spatial position x and time t, $\boldsymbol{f}(\Phi) = (f_1(\Phi), \ldots, f_N(\Phi))^{\mathrm{T}}$ is a vector of flux density functions, and $\boldsymbol{B}(\Phi)$ is a given $N \times N$ matrix function expressing a diffusive correction, where we allow that $\boldsymbol{B}(\Phi) = \boldsymbol{0}$ on a set of nonzero N-dimensional measure, so that (1.1) is possibly strongly degenerate. The system (1.1) is supplied with an initial condition and zero-flux or periodic boundary conditions. We focus on two applications, namely a model of polydisperse sedimentation where the diffusive correction accounts for sediment compressibility [4], and a version of the multiclass Lighthill-Whitham-Richards

*Department of Mathematics and Computer Science, University of Catania, 95125 Catania, Italy. E-Mail: boscarino@dmi.unict.it

†CI^{2}MA and Departamento de Ingeniería Matemática, Facultad de Ciencias Físicas y Matemáticas, Universidad de Concepción, Casilla 160-C, Concepción, Chile. E-Mail: rburger@ing-mat.udec.cl

‡Departament de Matemàtica Aplicada, Universitat de València, Av. Dr. Moliner 50, E-46100 Burjassot, Spain. E-Mail: mulet@uv.es

§Department of Mathematics and Computer Science, University of Catania, 95125 Catania, Italy. E-Mail: russo@dmi.unict.it

¶Departamento de Matemática, Facultad de Ciencias, Universidad del Bío-Bío, Casilla 5-C, Concepción, Chile. E-Mail: lvillada@ubiobio.cl

(MCLWR) traffic model [3, 29, 35, 42] where the diffusive correction describes the effects of reaction times and anticipation lengths. Both applications are examples of so-called multi-species kinematic flow models that involve N distinguishable species, which usually segregate with respect to a specific spatial direction (e.g., that of gravity).

Although there is no closed well-posedness theory for such strongly degenerate hyperbolic-parabolic systems, it is still plausible to perform simulations with appropriate numerical methods. Explicit schemes for hyperbolic systems of first-order conservation laws (i.e., $\boldsymbol{B} \equiv \boldsymbol{0}$) are widely used in many applications. When diffusion terms are present (i.e., $\boldsymbol{B} \not\equiv \boldsymbol{0}$), then an implicit treatment of these terms can overcome the drastic time step size restrictions imposed by the stability condition for explicit schemes applied to parabolic equations. This idea was used in [14] to introduce semi-implicit, so-called implicit-explicit (IMEX) Runge-Kutta (RK) schemes for (1.1), which involve the solution of highly nonlinear and nonsmooth systems of algebraic equations. This is achieved in [14] by a regularization of the nonsmooth diffusion coefficients combined with a suitable solver for the resulting nonlinear systems in an efficient way. While these techniques turned out to be robust and provide approximate solutions even when simpler methods (e.g., the Newton-Raphson (NR) method without line search) do not converge, their effort of implementation is considerable.

It is the purpose of this work to propose a new class of semi-implicit methods for the solution of (1.1), see [6], which are strongly inspired by partitioned Runge-Kutta (RK) methods [23]. To describe the main idea, assume that the semi-discrete formulation of (1.1) can be written in vector form as

$$\frac{\mathrm{d}\boldsymbol{\Phi}}{\mathrm{d}t} = -\frac{1}{\Delta x}(\Delta^{-}\boldsymbol{f})(\boldsymbol{\Phi}) + \frac{1}{\Delta x^2}\boldsymbol{\mathcal{B}}(\boldsymbol{\Phi})\boldsymbol{\Phi}, \tag{1.2}$$

where $\boldsymbol{\Phi} = (\Phi_1(t), \ldots, \Phi_M(t))^{\mathrm{T}}$ is the sought solution vector, where $\Phi_j(t)$ is the solution at spatial position x_j, $\Delta x := x_{j+1} - x_j$ for $j = 1, \ldots, M$ is the uniform grid spacing, $(\Delta^{-}\boldsymbol{f})(\boldsymbol{\Phi}) \in \mathbb{R}^{NM}$ denotes the vector of numerical flux vector differences associated with the discretization of $\partial_x \boldsymbol{f}(\Phi)$, and $\boldsymbol{\mathcal{B}}(\boldsymbol{\Phi}) \in \mathbb{R}^{(NM)\times(NM)}$ is a block tridiagonal matrix arising from the discretization of $\partial_x(\boldsymbol{B}(\Phi)\partial_x\Phi)$. The precise algebraic forms of $(\Delta^{-}\boldsymbol{f})(\boldsymbol{\Phi})$ and $\boldsymbol{\mathcal{B}}(\boldsymbol{\Phi})$ are provided in [14]. Here we emphasize that the matrix $\boldsymbol{\mathcal{B}}$ inherits its discontinuous dependence on $\boldsymbol{\Phi}$ from that of $\boldsymbol{B}$ on Φ.

The new approach is based on carefully distinguishing in (1.2) between stiff and non-stiff dependence on the solution vector $\boldsymbol{\Phi}$, and in choosing the time discretization by an implicit and an explicit RK scheme, respectively, of an IMEX pair of schemes accordingly. Roughly speaking, in the product $\boldsymbol{\mathcal{B}}(\boldsymbol{\Phi})\boldsymbol{\Phi}$ the occurrence of the solution $\boldsymbol{\Phi}$ within of $\boldsymbol{\mathcal{B}}(\boldsymbol{\Phi})$ is considered nonstiff, while that of the factor $\boldsymbol{\Phi}$ is considered stiff. Thus, the implicit treatment is applied only to that second factor, in contrast to [14] where the whole expression $\boldsymbol{\mathcal{B}}(\boldsymbol{\Phi})\boldsymbol{\Phi}$ is treated implicitly. This new approach does not require solutions for *nonlinear* systems (in contrast to the approach of [14]), since the new methods require only solving a discretized convection-diffusion equation with a *linear* diffusion term in which the matrix $\boldsymbol{\mathcal{B}}$ is given. We therefore address the new methods introduced herein as *linearly implicit* IMEX-RK methods, in contrast to the methods of [14] to which we refer as *nonlinearly implicit* IMEX-RK methods. Numerical examples demonstrate that the new linearly implicit methods, which are much easier to implement, approximate the same solutions as the nonlinearly implicit ones, and in many cases are more efficient.

1.2. Related work. First-order models of the type

$$\partial_t \Phi + \partial_x \boldsymbol{f}(\Phi) = \mathbf{0}, \quad \boldsymbol{f}(\Phi) = \big(\phi_1 v_1(\Phi), \dots, \phi_N v_N(\Phi)\big)^{\mathrm{T}}, \tag{1.3}$$

where Φ is the vector of partial densities or volume fractions and $v_1, \dots, v_N$ are given velocity functions, arise in models of polydisperse sedimentation [4, 10, 11, 21], multiclass vehicular traffic [3, 19, 42, 43], and the settling and creaming of emulsions and dispersions [1, 37]. A widely used velocity model for polydisperse sedimentation is the Masliyah-Lockett-Bassoon (MLB) model [30, 31]. On the other hand, the MCLWR model was introduced by Benzoni-Gavage and Colombo [3] and Wong and Wong [42]. For all these models, the eigenvectors and eigenvalues of the Jacobian $\mathcal{J}_{\boldsymbol{f}}(\Phi) = (\partial f_i(\Phi)/\partial \phi_j)_{1\le i,j\le N}$ are usually not available in closed form. However, for some of these models, $\mathcal{J}_{\boldsymbol{f}}(\Phi)$ is a low-rank perturbation of a diagonal matrix. In this case, and under determined circumstances, the eigenvalues of $\mathcal{J}_{\boldsymbol{f}}(\Phi)$ are real and interlace with the velocities v_i [10, 20]. This information is the key ingredient for the construction of efficient characteristic-wise weighted essentially non-oscillatory (WENO) schemes (see [39, 40]) for (1.3) [11, 19], which are employed herein to discretize the convective part of (1.1).

For models of polydisperse sedimentation, the diffusive terms leading to the form (1.1) describe the formation of compressible sediments (see [4]). In that paper, the system (1.1) was solved by the Kurganov-Tadmor (KT) explicit high-resolution central difference scheme [28]. On the other hand, the diffusively corrected version of the MCLWR traffic model is derived in [14].

Concerning the KT scheme, we remark that when a right-hand side is added to system (1.3), as in (1.1), one could discretize it in space, obtaining a method of lines that can be treated by some ODE solver. In the original approach of KT method, both convection and diffusion are treated explicitly [28, Sect. 4.2], and the time step is then restricted by stability rather than accuracy constrains. It is natural to treat the diffusion term implicitly, while maintaining the (possibly nonlinear) convection term explicit. This has been realised by adopting IMEX-RK schemes.

An IMEX-RK scheme consists in combining a RK scheme with an implicit discretization of the diffusive term and an explicit one for the convective term. To introduce the main idea, we consider the problem

$$\frac{\mathrm{d}\boldsymbol{\Phi}}{\mathrm{d}t} = C(\boldsymbol{\Phi}) + D(\boldsymbol{\Phi}), \tag{1.4}$$

where $C(\boldsymbol{\Phi})$ and $D(\boldsymbol{\Phi})$ are discretizations of the convective and diffusive terms, respectively. The stability restriction on the time step Δt that explicit schemes impose when applied to (1.4) is very severe (Δt must be proportional to the square Δx^2 of the grid spacing), due to the presence of $D(\boldsymbol{\Phi})$. The implicit treatment of both $C(\boldsymbol{\Phi})$ and $D(\boldsymbol{\Phi})$ would remove any stability restriction on Δt, but the upwind nonlinear discretization of $C(\boldsymbol{\Phi})$ that is needed for stability makes its implicit treatment extremely involved. In fact, numerical integrators that deal implicitly with $D(\boldsymbol{\Phi})$ and explicitly with $C(\boldsymbol{\Phi})$ can be used with a time step restriction dictated by the convective term alone [15]. These schemes have been profusely used for time-dependent problems involving stiff terms including hyperbolic systems with relaxation (see [5, 6, 8, 9, 34]). Moreover, several authors have proposed IMEX-RK schemes for the solution of semi-discretized partial differential equations (PDEs) [2, 24, 27, 34, 44].

1.3. Outline of the paper. The remainder of the paper is organized as follows. In Section 2 we describe the models that motivate our interest in the degenerate

convection-diffusion equation (1.1). To this aim, we first offer in Section 2.1 some general remarks on multispecies kinematic flow models. Then, in Section 2.2 we summarize Model 1, a model of polydisperse sedimentation of equal-density particles that form compressible sediments, and in Section 2.3 we outline Model 2, namely a multi-class version of the diffusively corrected kinematic traffic flow model introduced in [32] (see also [12]) for $N = 1$. In Section 3, which is at the core of the paper, both variants of semi-implicit IMEX-RK schemes are introduced. After providing some notation common to both versions (Section 3.2), we summarize in Section 3.3 the nonlinearly implicit IMEX-RK methods for solving the system (1.1) introduced in [14]. Section 3.4 is devoted to the new linearly implicit IMEX-RK methods. Numerical examples are presented in Section 4. We first state some preliminaries in Section 4.1, and compare in Examples 1 to 4 (Sections 4.2 and 4.3) the performance of the new linearly implicit IMEX-RK scheme with that of the nonlinearly implicit one of [14] for a test case of Model 1 with $N = 3$. The same model, but with a smooth initial datum, is used in Example 5 (Section 4.4) to assess the numerical order of accuracy of the linearly implicit IMEX-RK scheme. In Section 4.5 we present one test case for Model 2 (also with $N = 3$), for which the linearly implicit IMEX-RK scheme turns out to be more efficient than the nonlinearly implicit version. Finally, some concluding remarks are collected in Section 5.

2. Models.

2.1. Diffusively corrected multi-species kinematic flow models. The term "kinematic" means that the velocity v_i of species i is an explicit function of the vector Φ of the concentrations (volume fractions) ϕ_i of each species. Thus, standard multi-species kinematic flow models are given by systems of N scalar, in general nonlinear, first-order conservation laws (1.3). In this work we focus on multi-species flow models in which the velocities also depend on the spatial variation of Φ to account for additional effects such as sediment compressibility or drivers' reaction time and anticipation length in traffic flow. These corrections can be usually posed in such a way that the resulting system of PDEs has an extra, possibly strongly degenerate, diffusive term expressed by the right-hand side of (1.1).

2.2. Model 1: polydisperse sedimentation. The sedimentation of a suspension of equal-density particles belonging to N species with sizes $d_1 > d_2 > \cdots > d_N$ is a problem of interest in engineering applications, volcanology, and medicine. We let ϕ_i denote the local volume fraction of species i having size d_i, and define $\phi := \phi_1 + \cdots + \phi_N$. The evolution of $\Phi = \Phi(x,t)$ as a function of depth x and time t in a column of height $\mathcal{L}$ is then governed by the effects of hindered settling and sediment compressibility, which determine the convective and diffusive parts, respectively, of (1.1). This equation is now posed on the x-interval $(0,\mathcal{L})$ for $t > 0$, along with the initial condition $\Phi(x,0) = \Phi_0(x)$ for $0 \le x \le \mathcal{L}$, where Φ_0 is the given initial concentration distribution, and zero-flux boundary conditions, i.e.,

$$\boldsymbol{f}(\Phi) - \boldsymbol{B}(\Phi)\partial_x\Phi = \boldsymbol{0} \quad \text{for } x = 0 \text{ and } x = \mathcal{L}, \quad t > 0. \tag{2.1}$$

The flux density functions $f_1, \ldots, f_N$ are those of the MLB model [30, 31] given by

$$f_i(\Phi) = \mu\bar{\varrho}_{\mathrm{s}}\phi_i V(\phi)(1-\phi)(\delta_i - \boldsymbol{\delta}^{\mathrm{T}}\Phi), \quad i = 1, \ldots, N, \tag{2.2}$$

where $\mu > 0$ is a viscosity constant, $\bar{\varrho}_{\mathrm{s}} > 0$ is the solid mass density minus the fluid density, $\delta_i := d_i^2/d_1^2$, $\boldsymbol{\delta} := (\delta_1 = 1, \delta_2, \ldots, \delta_N)^{\mathrm{T}}$, and $V(\phi)$ is a hindered settling

function that is assumed to satisfy

$$V(\phi) \geq 0 \text{ for all } \phi, \quad V(0) = 1, \quad \text{and } V'(\phi) < 0 \text{ for } 0 \leq \phi < \phi_{\max}, \tag{2.3}$$

where $0 < \phi_{\max} \leq 1$ is a maximal total solids volume fraction. A typical expression is given by

$$V(\phi) = \begin{cases} (1-\phi)^{n_{\mathrm{RZ}}-2} & \text{for } 0 \leq \phi \leq \phi_{\max}, \\ 0 & \text{otherwise}, \end{cases} \tag{2.4}$$

where $n_{\mathrm{RZ}} > 2$ is the material-dependent Richardson-Zaki exponent [36]. For the flux (2.2), $\mathcal{J}_{\boldsymbol{f}}(\Phi)$ is a rank-two perturbation of a diagonal matrix. This property allows one to analyze hyperbolicity, to localize eigenvalues, and to eventually calculate the corresponding eigenvectors of $\mathcal{J}_{\boldsymbol{f}}(\Phi)$, see [10, 20]. The essential results are summarized in the following theorem, were $\mathcal{D}^0_{\phi_{\max}}$ is the interior of

$$\mathcal{D}_{\phi_{\max}} := \{\Phi \in \mathbb{R}^N : \phi_1 \geq 0, \ldots, \phi_N \geq 0,\, \phi \leq \phi_{\max}\}.$$

THEOREM 2.1 ([20]). *If $\delta_1 > \delta_2 > \cdots > \delta_N$ and $\Phi \in \mathcal{D}^0_{\phi_{\max}}$, then (1.1) with $\boldsymbol{B}(\Phi) = 0$ and $\boldsymbol{f}(\Phi)$ defined by (2.2), where the function V is assumed to satisfy (2.3), is strictly hyperbolic, i.e., $\mathcal{J}_{\boldsymbol{f}}(\Phi)$ has N distinct real eigenvalues $\lambda_1, \ldots, \lambda_N$. Moreover, the following so-called interlacing property holds:*

$$v_N + \gamma_1 + \cdots + \gamma_N < \lambda_N < v_N < \lambda_{N-1} < v_{N-1} < \cdots < \lambda_1 < v_1.$$

The diffusion matrix is given by

$$\boldsymbol{B}(\Phi) := (\alpha_{ij})_{1 \leq i,j \leq N}, \tag{2.5}$$

where for $N = 1$, we have for $\phi = \phi_1$ and $\delta = \delta_1 = 1$ the expression

$$\alpha = \alpha_{11} = \frac{\mu V(\phi)}{g}(1-\phi)^2 \sigma_{\mathrm{e}}'(\phi),$$

Here σ_{e} denotes the effective solid stress function, and σ_{e}' is its derivative. This function is assumed to satisfy

$$\sigma_{\mathrm{e}}(\phi), \sigma_{\mathrm{e}}'(\phi) \begin{cases} = 0 & \text{for } \phi \leq \phi_{\mathrm{c}}, \\ > 0 & \text{for } \phi > \phi_{\mathrm{c}}, \end{cases} \tag{2.6}$$

where ϕ_{c} is a critical concentration at which the particles touch each other. A typical function σ_{e} having these properties is given by

$$\sigma_{\mathrm{e}}(\phi) = \begin{cases} 0 & \text{for } \phi \leq \phi_{\mathrm{c}}, \\ \sigma_0\big((\phi/\phi_{\mathrm{c}})^k - 1\big) & \text{for } \phi > \phi_{\mathrm{c}}, \end{cases} \quad \sigma_0, k > 0. \tag{2.7}$$

For $N = 2$ the elements of the diffusion matrix $\boldsymbol{B}(\Phi)$ are given by

$$\alpha_{11} = \frac{\mu V(\phi)}{g\phi}\Big\{(1-\phi)\phi_1(1-\phi_1-\delta_2\phi_2)\sigma_{\mathrm{e}}'(\phi) \\ - \left[1 - \phi_1 - \frac{\phi_1}{\phi}(1-\phi_1-\delta_2\phi_2)\right]\sigma_{\mathrm{e}}(\phi)\Big\},$$

$$\alpha_{12} = \frac{\mu V(\phi)\phi_1}{g\phi}\Big\{(1-\phi)(1-\phi_1-\delta_2\phi_2)\sigma_{\mathrm{e}}'(\phi) + \Big[\delta_2 + \frac{1-\phi_1-\delta_2\phi_2}{\phi}\Big]\sigma_{\mathrm{e}}(\phi)\Big\},$$
$$\alpha_{21} = \frac{\mu V(\phi)\phi_2}{g\phi}\Big\{(1-\phi)(\delta_2-\phi_1-\delta_2\phi_2)\sigma_{\mathrm{e}}'(\phi) + \Big[1 - \frac{\delta_2-\phi_1-\delta_2\phi_2}{\phi}\Big]\sigma_{\mathrm{e}}(\phi)\Big\},$$
$$\alpha_{22} = \frac{\mu V(\phi)}{g\phi}\Big\{(1-\phi)\phi_2(\delta_2-\phi_1-\delta_2\phi_2)\sigma_{\mathrm{e}}'(\phi) - \Big[\delta_2 - \delta_2\phi_2 - \frac{\phi_2}{\phi}(\delta_2-\phi_1-\delta_2\phi_2)\Big]\sigma_{\mathrm{e}}(\phi)\Big\},$$

and for general N we have

$$\alpha_{ij} = \frac{\mu V(\phi)}{g\phi}\Big\{(1-\phi)\phi_i(\delta_i - \boldsymbol{\delta}^{\mathrm{T}}\Phi)\sigma_{\mathrm{e}}'(\phi) - \Big[\delta_i\delta_{ij} - \delta_j\phi_i - \frac{\phi_i}{\phi}(\delta_i - \boldsymbol{\delta}^{\mathrm{T}}\Phi)\Big]\sigma_{\mathrm{e}}(\phi)\Big\}, \quad i,j = 1,\dots,N, \tag{2.8}$$

where δ_{ij} is the standard Kronecker symbol. Clearly, (2.6) and (2.8) imply that

$$\boldsymbol{B}(\Phi) = \mathbf{0} \quad \text{for } \Phi \in \mathcal{D}_{\phi_{\mathrm{c}}}, \tag{2.9}$$

so (1.1) is usually strongly degenerate under the assumptions of Model 1, while on $\mathcal{D}^0_{\phi_{\max}}\backslash\mathcal{D}_{\phi_{\mathrm{c}}}$ the eigenvalues of $\boldsymbol{B}(\Phi)$ are positive, pairwise distinct, and satisfy an interlacing property with respect to certain known functions of ϕ [4, Th. 4.3].

2.3. Model 2: a diffusively corrected MCLWR model. We assume that $v_i^{\max}$ is the preferred velocity of vehicle class i, where $v_1^{\max} > v_2^{\max} > \cdots > v_N^{\max} > 0$. This preferential velocity is multiplied by a hindrance function $V = V(\phi)$, which describes drivers' attitude to reduce velocity in presence of other cars. If ϕ_i is the local density of class i, then the local velocity v_i of vehicles of class i is given by $v_i = v_i^{\max}V(\phi)$, where $\phi = \phi_1 + \cdots + \phi_N$ and V is a non-increasing function satisfying $V(0) = 1$, $V(\phi_{\max}) = 0$, and $V'(\phi) \le 0$ for $0 \le \phi \le \phi_{\max}$. Thus, the standard MCLWR model (without diffusive correction) is given by (1.3), where

$$f_i(\Phi) = \phi_i v_i^{\max} V(\phi), \quad i = 1,\dots,N. \tag{2.10}$$

We now assume that drivers of class i exhibit an anticipation distance L_i and a reaction time τ_i, $i = 1,\dots,N$, and follow Nelson [32] to show that these ingredients give rise to a diffusive correction. If $L_i > 0$, but $\tau_i = 0$, then the drivers' reaction does not depend on the value of ϕ seen at the same point (x,t), but rather on the density seen at position $x + L_i$ at time t. If $\tau_i > 0$, then the reaction at time t corresponds to information seen at time $t - \tau_i$, and we must subtract from the position $x + L_i$ the distance $v_i^{\max}V\tau_i$ traveled during a time interval of length τ_i. (For the moment we are not specific about the argument of V.) Thus, the reaction of the driver does not depend on $\phi(x,t)$, but on $p_i(x,t) := \phi(x + L_i - v_i^{\max}V\tau_i, t - \tau_i)$.

Next, we expand $V(p_i(x,t))$ around $\phi = \phi(x,t)$. Denoting $\tau := \max\{\tau_1,\dots,\tau_N\}$, $L := \max\{L_1,\dots,L_N\}$ and $\boldsymbol{v}^{\max} := (v_1^{\max},\dots,v_N^{\max})^{\mathrm{T}}$, we obtain (cf. [13, 14])

$$V(p_i(x,t)) = V(\phi) + V'(\phi)\big[\big(L_i - \tau_i v_i^{\max}V(\phi)\big)\partial_x\phi + \tau_i\partial_x\big(V(\phi)(\boldsymbol{v}^{\max})^{\mathrm{T}}\Phi\big)\big] + \mathcal{O}(\tau^2 + L^2).$$

Neglecting the $\mathcal{O}(\tau^2+L^2)$ term and inserting the result into the conservation equations

$$\partial_t\phi_i(x,t)+\partial_x\big(\phi_i(x,t)v_i(x,t)\big)=0,\quad v_i(x,t)=v_i^{\max}V\big(p_i(x,t)\big),\quad i=1,\dots,N,$$

we obtain a system of the form (1.1), where the components of the flux vector $\boldsymbol{f}(\Phi)$ are given by (2.10), and the diffusion matrix $\boldsymbol{B}(\Phi)$ is now given by (2.5) with

$$\begin{aligned}\alpha_{ij}(\Phi)=-V'(\phi)\big[L_i+\tau_i\big(V'(\phi)(\boldsymbol{v}^{\max})^{\mathrm{T}}\Phi+\big(v_j^{\max}-v_i^{\max}\big)V(\phi)\big)\big]\phi_i v_i^{\max},\\ 1\le i,j\le N.\end{aligned}\tag{2.11}$$

For the case $N=1$, we get $\alpha(\phi)=\alpha_{11}(\Phi)=-V'(\phi)[L_1+\tau_1V'(\phi)v_1^{\max}\phi]\phi v_1^{\max}$.

For traffic flow models we will use periodic boundary conditions corresponding to a circular road of length $\mathcal{L}$, namely

$$\Phi(0,t)=\Phi(\mathcal{L},t),\quad t>0.\tag{2.12}$$

The MCLWR model (1.1) with $\boldsymbol{B}\equiv 0$ is strictly hyperbolic and $\mathcal{J}_{\boldsymbol{f}}(\Phi)$ is a rank-one perturbation of a diagonal matrix [20]. Here the following theorem holds.

THEOREM 2.2 ([20]). *Consider the MCLWR model* (1.3), (2.10) *(i.e., without diffusive terms). If $\Phi\in\mathcal{D}_1^0$, then the Jacobian $\mathcal{J}_{\boldsymbol{f}}(\Phi)$ has N distinct real eigenvalues $\lambda_1,\dots,\lambda_N$, and the following interlacing property holds:*

$$v_N^{\max}+V'(\phi)(\boldsymbol{v}^{\max})^{\mathrm{T}}\Phi<\lambda_N<v_N^{\max}<\lambda_{N-1}<v_{N-1}^{\max}<\cdots<v_2^{\max}<\lambda_1<v_1^{\max}.$$

In contrast to Model 1, here the conditions under which $\boldsymbol{B}(\Phi)$ has eigenvalues with positive real part for all $\Phi\in\mathcal{D}_{\phi_{\max}}$ depend in a delicate way on the choices of the non-negative parameters $v_i^{\max}$, τ_i and L_i, see [13, 14] for details. We will consider only test cases for which these properties are clearly established.

In the case $N=1$, Nelson [32] (cf. [12]) suggests to employ

$$L=L(\phi)=\max\big\{(v_{\max}V(\phi))^2/(2a),L_{\min}\big\},\tag{2.13}$$

where the first argument is the distance required to decelerate to full stop from speed $v_{\max}V(\phi)$ at deceleration a, and $L_{\min}>0$ is a minimal anticipation distance. In the multi-class case we could define L_i, for instance, by (2.13) with $v_{\max}$ replaced by $v_i^{\max}$. However, in our numerical experiments, we select L_i and τ_i constant, to ensure that (1.1) is hyperbolic-parabolic (see [14, section 2.4] for a discussion of this point).

A common choice of $V=V(\phi)$ in traffic modelling is the model

$$V(\phi)=V_{\mathrm{DG}}(\phi)=\min\{1,-C\ln\phi\}\tag{2.14}$$

due to Dick and Greenberg [18, 22], where C is a positive constant. Since

$$\begin{cases}V(\phi)=1,\ V'(\phi)=0 & \text{for } 0\le\phi\le\phi_{\mathrm{c}}=\exp(-1/C),\\ V(\phi)=-C\ln\phi,\ V'(\phi)=-C/\phi & \text{for } \phi_{\mathrm{c}}<\phi<1,\end{cases}\tag{2.15}$$

using the model (2.14) in (2.11) means that (2.9) also holds for Model 2, i.e., (1.1) again becomes strongly degenerate. We mention that besides this consequence of the particular choice (2.14), there is also an alternative, independent justification of (2.9) in traffic modelling based on interpreting ϕ_{c} as a perception threshold [38].

Finally, we remark that for both Model 1 with $\sigma_{\mathrm{e}}(\phi)$ defined by (2.7) and Model 2 with $V(\phi)$ defined by (2.14), the diffusion matrix $\boldsymbol{B}(\Phi)$ is discontinuous at $\phi = \phi_{\mathrm{c}}$. This property is explicitly included in the well-posedness analysis available for (1.1) in the *scalar* case (cf., e.g., [25, 26]). It is required that if the right-hand side of the PDE is written as $A(\phi)_{xx}$, where $A = A(\phi)$ is a primitive of the diffusion function $B(\phi)$ (to which $B(\Phi)$ reduces in the scalar case), then A should be (locally) Lipschitz continuous and nondecreasing, which is satisfied if $B(\phi)$ is bounded and, for instance, piecewise continuous.

3. Numerical schemes.

3.1. Spatial discretization. The discretization $\frac{1}{\Delta x}(\Delta^- \boldsymbol{f})(\boldsymbol{\Phi})$ of the convective term $\partial_x \boldsymbol{f}(\Phi)$ is computed using the WENO-SPEC scheme (see [11] for full details). The numerical fluxes are obtained by fifth-order WENO reconstructions of characteristic fluxes, following Shu and Osher's technique [41]. The computation of the characteristic information is based on the interlacing property, see Theorems 2.1 and 2.2. (The acronym "WENO-SPEC" introduced in [11] emphasizes the use of spectral information for this class of WENO schemes, in contrast to easier-to-implement, but less efficient, component-wise schemes, which are not considered herein.)

For the discretization of the diffusive term $\partial_x(\boldsymbol{B}(\Phi)\partial_x\Phi)$ we limit ourselves to second-order schemes, since solutions are not smooth, and use the following discretization (see [14] for full details):

$$\partial_x\big(\boldsymbol{B}(\Phi)\partial_x\Phi\big)(x_i,t) \approx \frac{1}{\Delta x^2}\big(\boldsymbol{B}_{i-1/2}\boldsymbol{\Phi}_{i-1} - (\boldsymbol{B}_{i-1/2}+\boldsymbol{B}_{i+1/2})\boldsymbol{\Phi}_i + \boldsymbol{B}_{i+1/2}\boldsymbol{\Phi}_{i+1}\big)(t),$$

$$\boldsymbol{B}_{i+1/2} = \boldsymbol{B}_{i+1/2}(\boldsymbol{\Phi}_i,\boldsymbol{\Phi}_{i+1}) := \frac{1}{2}\big(\boldsymbol{B}(\boldsymbol{\Phi}_i)+\boldsymbol{B}(\boldsymbol{\Phi}_{i+1})\big),$$

where $\boldsymbol{\Phi}_i(t) \approx \Phi(x_i,t) \in \mathbb{R}^N$. The terms $\boldsymbol{B}_{i\pm1/2}\boldsymbol{\Phi}_{i\pm1}$ for $i = 1$ and $i = M$ are modified according to the boundary conditions.

With the notation $\boldsymbol{\Phi} = (\boldsymbol{\Phi}_1^{\mathrm{T}},\dots\boldsymbol{\Phi}_M^{\mathrm{T}})^{\mathrm{T}} \in \mathbb{R}^{MN}$, we can define the $M\times M$ block tridiagonal matrix $\boldsymbol{\mathcal{B}} = \boldsymbol{\mathcal{B}}(\boldsymbol{\Phi})$, with blocks of size $N\times N$, as

$$\boldsymbol{\mathcal{B}}_{i,i} = -(\boldsymbol{B}_{i-1/2}+\boldsymbol{B}_{i+1/2}), \quad \boldsymbol{\mathcal{B}}_{i,i-1} = \boldsymbol{B}_{i-1/2}, \quad \boldsymbol{\mathcal{B}}_{i,i+1} = \boldsymbol{B}_{i+1/2},$$

for which we have

$$\big(\boldsymbol{\mathcal{B}}(\boldsymbol{\Phi})\boldsymbol{\Phi}\big)_i(t) = \big(\boldsymbol{B}_{i-1/2}\boldsymbol{\Phi}_{i-1} - (\boldsymbol{B}_{i-1/2}+\boldsymbol{B}_{i+1/2})\boldsymbol{\Phi}_i + \boldsymbol{B}_{i+1/2}\boldsymbol{\Phi}_{i+1}\big)(t).$$

3.2. Notation. A good time integrator for the system (1.2) is represented by semi-implicit IMEX-RK schemes, where the convective term is treated explicitly and the diffusive term is treated implicitly. The corresponding pair of Butcher arrays of IMEX-RK methods is given by

$$\begin{array}{c|c} \tilde{\boldsymbol{c}} & \tilde{\boldsymbol{A}} \\ \hline & \tilde{\boldsymbol{b}}^{\mathrm{T}} \end{array} \qquad \begin{array}{c|c} \boldsymbol{c} & \boldsymbol{A} \\ \hline & \boldsymbol{b}^{\mathrm{T}} \end{array},$$

where the $s\times s$ lower triangular matrices $\tilde{\boldsymbol{A}} = (\tilde{a}_{ij})$ (with $\tilde{a}_{ij} = 0$ for all $j \geq i$) and $\boldsymbol{A} = (a_{ij})$ are the matrices of the explicit and implicit parts of the method, respectively, while $\tilde{\boldsymbol{b}} = (\tilde{b}_1,\dots,\tilde{b}_s)^{\mathrm{T}}$, $\tilde{\boldsymbol{c}} = (\tilde{c}_1,\dots,\tilde{c}_s)^{\mathrm{T}}$, $\boldsymbol{b} = (b_1,\dots,b_s)^{\mathrm{T}}$ and $\boldsymbol{c} = (c_1,\dots,c_s)^{\mathrm{T}}$ are s-dimensional vectors of real coefficients, and $\tilde{\boldsymbol{c}}$ and $\boldsymbol{c}$ are given by the usual relations

$$\tilde{c}_i = \sum_{j=1}^{i-1}\tilde{a}_{ij}, \quad c_i = \sum_{j=1}^{i} a_{ij}, \quad i = 1,\dots,s.$$

3.3. Nonlinearly implicit IMEX-RK methods. To describe the nonlinearly implicit IMEX-RK method for solving (1.1) introduced in [14], we rewrite the semidiscrete formulation (1.2) in the form (1.4), where we define

$$C(\mathbf{\Phi}) := -\frac{1}{\Delta x}(\Delta^- \boldsymbol{f})(\mathbf{\Phi}), \quad D(\mathbf{\Phi}) := \frac{1}{\Delta x^2}\boldsymbol{\mathcal{B}}(\mathbf{\Phi})\mathbf{\Phi}.$$

The simplest IMEX scheme for the approximation of (1.2) is

$$\mathbf{\Phi}^{n+1} = \mathbf{\Phi}^n - \frac{\Delta t}{\Delta x}(\Delta^- \boldsymbol{f})(\mathbf{\Phi}^n) + \frac{\Delta t}{\Delta x^2}\boldsymbol{\mathcal{B}}(\mathbf{\Phi}^{n+1})\mathbf{\Phi}^{n+1}, \tag{3.1}$$

where $\mathbf{\Phi}^n$ denotes the approximate value of $\mathbf{\Phi}(t)$ at $t = t^n$. For general pairs of RK schemes, the computations of a nonlinearly implicit IMEX-RK scheme necessary to advance an $\mathbf{\Phi}^n$ from time t^n to $t^{n+1} = t^n + \Delta t$ are given in Algorithm 3.1 [2, 34]:

ALGORITHM 3.1 (Nonlinearly implicit IMEX-RK scheme [14]).

Input: approximate solution vector $\mathbf{\Phi}^n$ for $t = t_n$

do $i = 1, \dots, s$

solve for $\mathbf{\Phi}^{(i)}$ the nonlinear equation

$$\mathbf{\Phi}^{(i)} = \mathbf{\Phi}^n + \Delta t\left(\sum_{j=1}^{i-1} a_{ij}K_j + a_{ii}D\big(\mathbf{\Phi}^{(i)}\big) + \sum_{j=1}^{i-1}\tilde{a}_{ij}\tilde{K}_j\right)$$

$K_i \leftarrow D(\mathbf{\Phi}^{(i)})$

$\tilde{K}_i \leftarrow C(\mathbf{\Phi}^{(i)})$

enddo

$$\mathbf{\Phi}^{n+1} \leftarrow \mathbf{\Phi}^n + \Delta t\sum_{j=1}^{s} b_jK_j + \Delta t\sum_{j=1}^{s}\tilde{b}_j\tilde{K}_j$$

Output: approximate solution vector $\mathbf{\Phi}^{n+1}$ for $t = t^{n+1} = t^n + \Delta t$.

Algorithm 3.1 requires solving for the vector $\boldsymbol{u} = \mathbf{\Phi}^{(i)} \in \mathbb{R}^{MN}$ a nonlinear system of NM scalar equations of the following form

$$\mathbf{\Psi}_i(\boldsymbol{u}) := \boldsymbol{u} - a_{ii}\Delta t D\big(\boldsymbol{u}\big) - \boldsymbol{r}_i = \mathbf{0}, \quad i = 1, \dots, s, \tag{3.2}$$

where $\boldsymbol{r}_i \in \mathbb{R}^{MN}$ is given by

$$\boldsymbol{r}_i = \mathbf{\Phi}^n + \Delta t\left(\sum_{j=1}^{i-1} a_{ij}K_j + \sum_{j=1}^{i-1}\tilde{a}_{ij}\tilde{K}_j\right).$$

For the sake of simplicity, we denote $\mathbf{\Psi} = \mathbf{\Psi}_i$ for $i = 1, \dots, s$ in the rest of the paper.

To approximately solve (3.2) by the NR iterative method we must require the coefficients of the matrix function $\boldsymbol{B}$, and therefore those of $\boldsymbol{\mathcal{B}}$, to be at least continuously differentiable [33, p. 311]. However, Models 1 and 2 do not naturally satisfy this assumption. Therefore, according to the description of nonlinearly implicit IMEX-RK schemes in [14], $\boldsymbol{B}$ is replaced by a smooth approximation $\boldsymbol{B}_\varepsilon$, and we denote the corresponding version of $\boldsymbol{\mathcal{B}}$ by $\boldsymbol{\mathcal{B}}_\varepsilon$, where $\boldsymbol{B}_\varepsilon \to \boldsymbol{B}$ and $\boldsymbol{\mathcal{B}}_\varepsilon \to \boldsymbol{\mathcal{B}}$ as $\varepsilon \to 0$. Note that the purpose of this approximation is to create smoothness, but not to convert the problem into a uniformly parabolic one. Then, we denote by $\mathbf{\Psi}_\varepsilon(\boldsymbol{u})$ the function (3.2), where $\boldsymbol{\mathcal{B}}(\boldsymbol{u})$ has been replaced by $\boldsymbol{\mathcal{B}}_\varepsilon(\boldsymbol{u})$. The function $\mathbf{\Psi}_\varepsilon$ is highly nonlinear for small ε, in the sense that the second derivative of $\mathbf{\Psi}_\varepsilon$ is much larger than its first derivative. Therefore, as is discussed in [14], by Kantorovich's theorem (see [17]), the region of guaranteed convergence shrinks when $\varepsilon \to 0$. On the other hand, the linearity of $\mathbf{\Psi}_\varepsilon$ behaves in the opposite way when increasing ε, so the region of guaranteed

convergence of the NR method increases. In light of these observations, we propose in [14] a strategy similar to that of [16] to efficiently solve $\boldsymbol{\Psi}_\varepsilon(\boldsymbol{u}) = \mathbf{0}$ for a prescribed $\varepsilon = \varepsilon_{\min}$. This strategy proceeds as follows: If $\boldsymbol{u}_\varepsilon$ is a solution of $\boldsymbol{\Psi}_\varepsilon(\boldsymbol{u}_\varepsilon) = \mathbf{0}$, then $\boldsymbol{u}_\varepsilon$ is used as an initial datum for approximating the solution of $\boldsymbol{\Psi}_{\varepsilon'}(\boldsymbol{u}) = \mathbf{0}$ for $\varepsilon' < \varepsilon$ by the NR method with a line search strategy [17]. This process is started with a sufficiently large value ε_0 and it is performed until a solution $\boldsymbol{\Psi}_{\varepsilon_{\min}}(\boldsymbol{u}) = \mathbf{0}$ is obtained. This process is summarized in Algorithm 4.1 of [14].

3.4. Linearly implicit IMEX-RK methods. The nonlinearly implicit IMEX-RK schemes proposed in [14], and whose simplest variant is (3.1), require solving a nonlinear system of NM scalar equations, as is detailed in Algorithm 3.1. To overcome this excessive numerical work for the solution of the nonlinear system (3.2), an essential gain is obtained by the following approach. We rewrite the semidiscrete formulation (1.2) in the form

$$\frac{\mathrm{d}\boldsymbol{\Phi}}{\mathrm{d}t} = \mathcal{C}(\boldsymbol{\Phi}) + \mathcal{D}(\boldsymbol{\Phi}, \boldsymbol{\Phi}) \tag{3.3}$$

with

$$\mathcal{C}(\boldsymbol{\Phi}) := -\frac{1}{\Delta x}(\Delta^- \boldsymbol{f})(\boldsymbol{\Phi}), \quad \mathcal{D}(\boldsymbol{\Phi}^*, \boldsymbol{\Phi}) := \frac{1}{\Delta x^2}\boldsymbol{\mathcal{B}}(\boldsymbol{\Phi}^*)\boldsymbol{\Phi}.$$

Here the idea is to distinguish in the system (3.3) between stiff and nonstiff dependence on the variable $\boldsymbol{\Phi}$. More precisely, by (3.3) we consider

$$\frac{\mathrm{d}\boldsymbol{\Phi}}{\mathrm{d}t} = \mathcal{C}(\boldsymbol{\Phi}^*) + \mathcal{D}(\boldsymbol{\Phi}^*, \boldsymbol{\Phi}) =: \mathcal{K}(\boldsymbol{\Phi}^*, \boldsymbol{\Phi}),$$

where $\boldsymbol{\Phi}^*$ is treated explicitly as argument of $\boldsymbol{f}$ and $\boldsymbol{\mathcal{B}}$, while $\boldsymbol{\Phi}$ is implicit in the term to which $\boldsymbol{\mathcal{B}}$ is applied.

Then the step from t^n to $t^{n+1} = t^n + \Delta t$ of the new linearly implicit IMEX-RK scheme is given by the following algorithm.

ALGORITHM 3.2 (Linearly implicit IMEX-RK scheme).

Input: approximate solution vector $\boldsymbol{\Phi}^n$ for $t = t^n$

do $i = 1, \ldots, s$

compute the stage values:

$$\boldsymbol{\Phi}^{*(i)} \leftarrow \boldsymbol{\Phi}^n + \Delta t \sum_{j=1}^{i-1} \tilde{a}_{ij} K_j$$

$$\hat{\boldsymbol{\Phi}}^{(i)} \leftarrow \boldsymbol{\Phi}^n + \Delta t \sum_{j=1}^{i-1} a_{ij} K_j$$

solve for K_i the linear equation

$$K_i = \mathcal{C}\big(\boldsymbol{\Phi}^{*(i)}\big) + \mathcal{D}\Big(\boldsymbol{\Phi}^{*(i)}, \hat{\boldsymbol{\Phi}}^{(i)} + \Delta t a_{ii} K_i\Big), \tag{$*$}$$

where

$$\mathcal{D}\Big(\boldsymbol{\Phi}^{*(i)}, \hat{\boldsymbol{\Phi}}^{(i)} + \Delta t a_{ii} K_i\Big) = \frac{1}{\Delta x^2}\boldsymbol{\mathcal{B}}\big(\boldsymbol{\Phi}^{*(i)}\big)\Big(\hat{\boldsymbol{\Phi}}^{(i)} + \Delta t a_{ii} K_i\Big)$$

enddo

$$\boldsymbol{\Phi}^{n+1} \leftarrow \boldsymbol{\Phi}^n + \Delta t \sum_{j=1}^{s} b_j K_j \tag{$**$}$$

Output: approximate solution vector $\boldsymbol{\Phi}^{n+1}$ for $t = t^{n+1} = t^n + \Delta t$.

Thus, the simplest first-order linearly implicit IMEX scheme for the approximation of (3.3) is

$$\boldsymbol{\Phi}^{n+1} = \boldsymbol{\Phi}^n - \frac{\Delta t}{\Delta x}(\Delta^- \boldsymbol{f})(\boldsymbol{\Phi}^n) + \frac{\Delta t}{\Delta x^2}\boldsymbol{\mathcal{B}}(\boldsymbol{\Phi}^n)\boldsymbol{\Phi}^{n+1}.$$

Concerning $(**)$ we observe that for the final numerical solution, we require, in particular,

$$\boldsymbol{\Phi}^{*,n+1} = \boldsymbol{\Phi}^{n+1},$$

which is guaranteed by imposing the condition

$$b_i = \tilde{b}_i \quad \text{for } i = 1, \ldots, s, \tag{3.4}$$

and no duplication of variables is needed in the computation of the numerical solution (for more details see [6, 7]).

Furthermore, we note that this new approach includes Zhong's method [44]. In fact, the theory developed in [44] for additive semi-implicit RK methods can be extended in a straightforward manner to these methods. In [44] the system of first-order ordinary differential equations is of the form

$$\frac{\mathrm{d}\Phi}{\mathrm{d}t} = \mathcal{F}(\Phi) + \mathcal{G}(\Phi).$$

Then, by setting $\mathcal{K}(\Phi^*, \Phi) = \mathcal{F}(\Phi^*) + \mathcal{G}(\Phi)$ we obtain for the numerical method

$$\begin{aligned} k_i &= \mathcal{K}\left(\Phi^n + \Delta t \sum_{j=1}^{i-1} \tilde{a}_{ij} k_j, \Phi^n + \Delta t \sum_{j=1}^{i-1} a_{ij} k_j + \Delta t a_{ii} k_i\right) \\ &= \mathcal{F}\left(\Phi^n + \Delta t \sum_{j=1}^{i-1} \tilde{a}_{ij} k_j\right) + \mathcal{G}\left(\Phi^n + \Delta t \sum_{j=1}^{i-1} a_{ij} k_j + \Delta t a_{ii} k_i\right) \end{aligned}$$

for $i = 1, \ldots, s$ and for the numerical solution

$$\Phi^{n+1} = \Phi^n + \Delta t \sum_{i=1}^{s} b_i\, k_i,$$

which are exactly the formulas proposed by Zhong [44].

The decisive advantage of the new linearly implicit approach for computing the numerical solution of system (3.3) is obvious: we do not require solutions for any nonlinear system, as for example in [14] for the nonlinear system (3.7) (of that paper). In this new approach, the system $(*)$ is linear in K_i and the numerical solution can be obtained by solving a convection-diffusion equation with a linear diffusion term in which the matrix function $\boldsymbol{B}$, and therefore $\boldsymbol{\mathcal{B}}$, is computed explicitly.

As an example, we propose a classical second-order IMEX-RK scheme that satisfies (3.4), namely the following scheme IMEX-SSP2(3,3,2) introduced in [34]:

$$\begin{array}{c|c} \tilde{\boldsymbol{c}} & \tilde{\boldsymbol{A}} \\ \hline & \tilde{\boldsymbol{b}}^{\mathrm{T}} \end{array} = \begin{array}{c|ccc} 0 & 0 & 0 & 0 \\ 1/2 & 1/2 & 0 & 0 \\ 1 & 1/2 & 1/2 & 0 \\ \hline & 1/3 & 1/3 & 1/3 \end{array}, \qquad \begin{array}{c|c} \boldsymbol{c} & \boldsymbol{A} \\ \hline & \boldsymbol{b}^{\mathrm{T}} \end{array} = \begin{array}{c|ccc} 1/4 & 1/4 & 0 & 0 \\ 1/4 & 0 & 1/4 & 0 \\ 1 & 1/3 & 1/3 & 1/3 \\ \hline & 1/3 & 1/3 & 1/3 \end{array}. \tag{3.5}$$

4. Numerical results.

4.1. Preliminaries. In the following examples, we solve (1.1) numerically for $0 \le t \le T$ and $0 \le x \le \mathcal{L}$ for Models 1 and 2. We compare numerical results obtained by the nonlinearly implicit IMEX-RK scheme for the coefficients (3.5), described in Section 3.3 and [14], which is denoted here by NI-IMEX-SSP2 (where we skip "(3,3,2)" for brevity and since we do not vary herein the RK coefficients) with those obtained by the new linearly implicit IMEX-RK scheme of Section 3.4, denoted by LI-IMEX-SSP2, and by the explicit Kurganov-Tadmor (KT) method [28].

For each model, the x-interval $[0, \mathcal{L}]$ is subdivided into M subintervals of length $\Delta x = \mathcal{L}/M$. We denote by Δt the time step used to advance the numerical solution from time $t = t^n$ to $t^{n+1} = t^n + \Delta t$ and by Φ_j^n the vector of numerical solutions associated with cell $[j\Delta x, (j+1)\Delta x]$, $j = 0, \ldots, M-1$, at time t^n. For each iteration, the time step Δt is determined by the following formula (derived from a linearized CFL condition):

$$\frac{\Delta t}{\Delta x} \max_{1\le j\le M} \varrho\big(\mathcal{J}_{\boldsymbol{f}}(\Phi_j^n)\big) + \frac{\Delta t}{2\Delta x^2} \max_{1\le j\le M} \varrho\big(\boldsymbol{B}(\Phi_j^n)\big) = C_{\mathrm{cfl}_1}$$

for the KT scheme and

$$\frac{\Delta t}{\Delta x} \max_{1\le j\le M} \varrho\big(\mathcal{J}_{\boldsymbol{f}}(\Phi_j^n)\big) = C_{\mathrm{cfl}_2}$$

for the semi-implicit schemes, where $\varrho(\cdot)$ is the spectral radius. In the numerical examples we choose C_{cfl_*} as the largest multiple of 0.05 that yields oscillation-free numerical solutions.

For comparison purposes, we compute reference solution for numerical tests by the KT scheme with $M_{\mathrm{ref}} = 25600$ cells. To be consistent with our previous work [14], we compute approximate L^1 errors at different times for each scheme as follows. We denote by $(\phi_{j,i}^M(t))_{j=1}^M$ and $(\phi_{l,i}^{\mathrm{ref}}(t))_{l=1}^{M_{\mathrm{ref}}}$ the numerical solution for the i-th component at time t calculated with M and M_{ref} cells, respectively. We use cubic interpolation from the reference grid to the M-cell grid to compute $\tilde{\phi}_{j,i}^{\mathrm{ref}}(t)$ for $j = 1, \ldots, M$. We calculate the total approximate L^1 error at time t assciated with the numerical solution on the M-cell grid by

$$e_M^{\mathrm{tot}}(t) := \frac{1}{M} \sum_{i=1}^{N} \sum_{j=1}^{M} \big|\tilde{\phi}_{j,i}^{\mathrm{ref}}(t) - \phi_{j,i}^M(t)\big|. \tag{4.1}$$

Based on the errors defined by (4.1), we may calculate a numerical order of convergence from pairs of total approximate L^1 errors $e_M^{\mathrm{tot}}(t)$ and $e_{2M}^{\mathrm{tot}}(t)$ by

$$\theta_M(t) := \log_2\big(e_M^{\mathrm{tot}}(t)/e_{2M}^{\mathrm{tot}}(t)\big). \tag{4.2}$$

To demonstrate that our way of calculating approximate errors and estimating convergence rates leads to conclusions that are independent of the particular reference solution, we employ in one case (Example 5) an alternative way of calculating approximate errors and convergence rates; namely, we use cubic interpolation from the grid of $2M$ cells that of M cells grid to compute the quantities

$$\tilde{\phi}_{j,i}^M(t) = \frac{9}{16}\big(\phi_{2j,i}^{2M} + \phi_{2j-1,i}^{2M}\big) - \frac{1}{16}\big(\phi_{2j+1,i}^{2M} + \phi_{2j-2,i}^{2M}\big), \quad j = 1, \ldots, M. \tag{4.3}$$

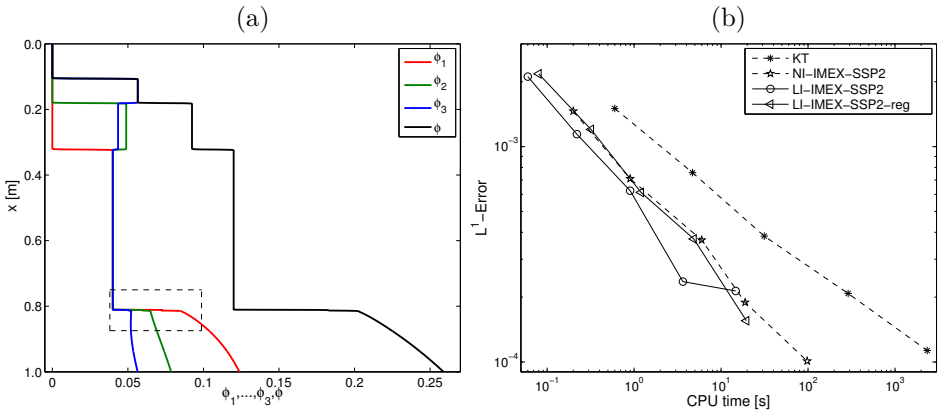

FIG. 4.1. *Example 1 (Model 1): (a) numerical solution obtained by LI-IMEX-SSP2 scheme at simulated time* $T = 4000\,\mathrm{s}$ *and* $\Delta x = 1/1600$*, (b) efficiency plot obtained for discretization levels* $\Delta x = 1/M$ *with* $M = 100$*,* 200*,* 400*,* 800 *and* 1600*.*

We then calculate an alternative (to (4.1)) total approximate L^1 error by

$$\hat{e}_M^{\mathrm{tot}}(t) := \frac{1}{M}\sum_{i=1}^{N}\sum_{j=1}^{M}\big|\tilde{\phi}_{j,i}^M(t) - \phi_{j,i}^M(t)\big|. \tag{4.4}$$

An alternative numerical order of convergence can then be computed by

$$\hat{\theta}_M(t) := \log_2\big(\hat{e}_M^{\mathrm{tot}}(t)/\hat{e}_{2M}^{\mathrm{tot}}(t)\big). \tag{4.5}$$

(Note carefully that $\hat{\theta}_M(t)$ is calculated from the three numerical solutions calculated on grids with M, $2M$, and $4M$ cells.) Since the scheme is second-order accurate for smooth solutions, an estimate of the (unknown) total exact L^1 error

$$e_M^{\mathrm{tot},*}(t) := \frac{1}{M}\sum_{i=1}^{N}\sum_{j=1}^{M}\big|\phi_i(x_j,t) - \phi_{j,i}^M(t)\big| \tag{4.6}$$

is given by

$$e_M^{\mathrm{tot},*}(t) \approx \tilde{e}_M^{\mathrm{tot}}(t) := \frac{4}{3}\hat{e}_M^{\mathrm{tot}}(t). \tag{4.7}$$

The motivation of (4.3)–(4.7) is briefly recalled in the Appendix.

4.2. Example 1: Model 1 with $N = 3$, comparison of LI- and NI-IMEX-SSP2 schemes. We employ Model 1 to simulate the settling of a tridisperse ($N = 3$) suspension forming a compressible sediment [4]. The mixture is described by the model functions (2.2), (2.4), (2.7) and (2.8) with $\phi_{\max} = 0.66$, $n_{\mathrm{RZ}} = 4.7$, $\sigma_0 = 180\,\mathrm{Pa}$, $\phi_{\mathrm{c}} = 0.2$, $k = 2$, $\mu_{\mathrm{f}} = 10^{-3}\,\mathrm{Pa\,s}$, $d = 1.19\times10^{-5}\,\mathrm{m}$, $\overline{\rho}_{\mathrm{s}} = 1800\,\mathrm{kg/m^3}$, and $g = 9.81\,\mathrm{m/s^2}$. The initial concentration is $\Phi_0 = (0.04, 0.04, 0.04)^{\mathrm{T}}$ in a vessel of height $\mathcal{L} = 1\,\mathrm{m}$ with normalized squared particle sizes $\boldsymbol{\delta} = (1, 0.5, 0.25)^{\mathrm{T}}$. Here and in Examples 2 to 5 we employ the zero-flux boundary conditions (2.1).

We compare numerical results obtained by schemes LI-IMEX-SSP2, NI-IMEX-SSP2 and KT at simulated time $T = 4000\,\mathrm{s}$. For the scheme NI-IMEX-SSP2, we

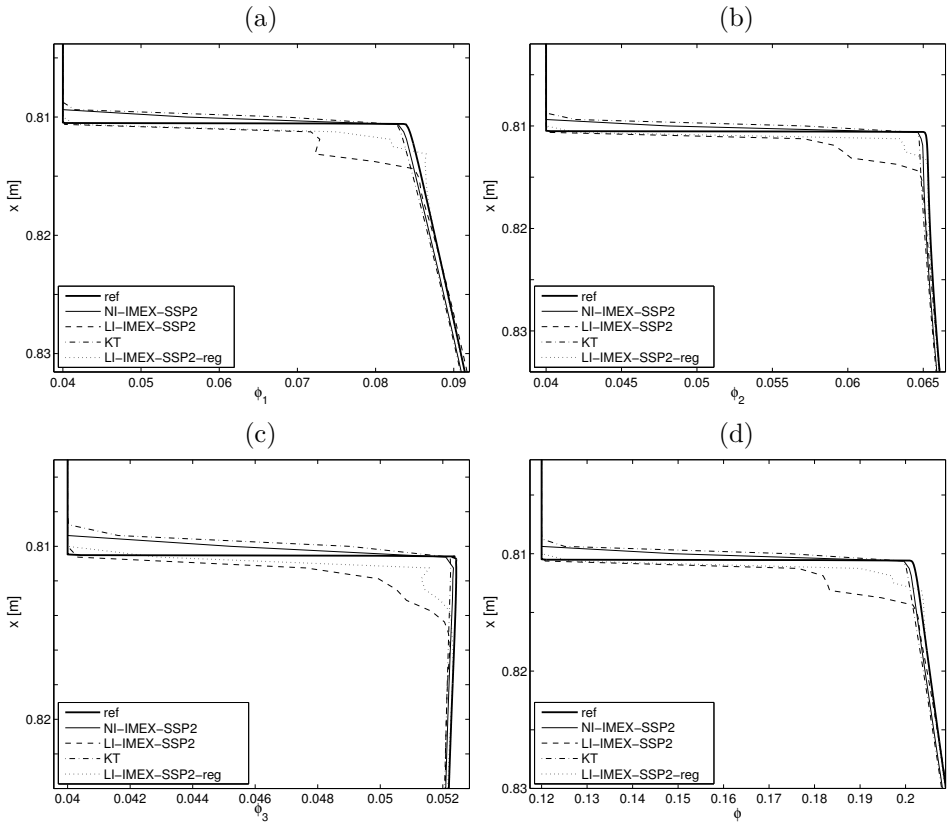

FIG. 4.2. *Example 1 (Model 1): enlarged views of the numerical solution of Figure 4.1 (a) near the parabolic-hyperbolic interface ($\phi = \phi_c$).*

solve the nonlinear system by Algorithm 4.1 of [14], where the regularization $\boldsymbol{B}_\varepsilon$ of the original diffusion matrix $\boldsymbol{B}$ is achieved by replacing the function σ_e in (2.8) by

$$\sigma_e(\phi;\varepsilon) = \sigma_e(\phi)\exp\bigl(-\varepsilon/(\phi-\phi_c)^2\bigr), \quad \varepsilon > 0,$$

where ε decreases gradually from $\varepsilon_0 = 10^{-4}$ to $\varepsilon_{\min} = 10^{-6}$, tol $= 10^{-8}$, while the LI-IMEX-SSP2 and KT schemes are applied without regularization of the diffusive term (this also includes the reference solution). For the schemes NI-IMEX-SSP2 and LI-IMEX-SSP2 we use $C_{\mathrm{cfl}_2} = 0.7$, and for the KT scheme, $C_{\mathrm{cfl}_1} = 0.25$.

The scheme LI-IMEX-SSP2 executes faster than NI-IMEX-SSP2 since the former needs to solve only one linear system per RK stage, whereas the latter has to solve many during the nonlinear solves in Algorithm 4.1 of [14]. Figure 4.1 (a) show that, in general, the sedimentation process is approximated adequately by the LI-IMEX-SSP2 scheme, but some overshoots appear close to the parabolic-hyperbolic interface $\phi = \phi_c$. These glitches do not disappear upon refinement. Therefore, the approximation errors with respect to the reference solution (computed without ε regularization) are larger than for NI-IMEX-SSP2, see Figure 4.1 (b). Enlarged views of the box area in Figure 4.1 (a) are displayed in Figure 4.2 for each component.

Another strategy, denoted by LI-IMEX-SSP2-reg, is to use the LI-IMEX-SSP2 directly applied to the regularized diffusion term with $\varepsilon_{\min} = 10^{-6}$. Numerical results

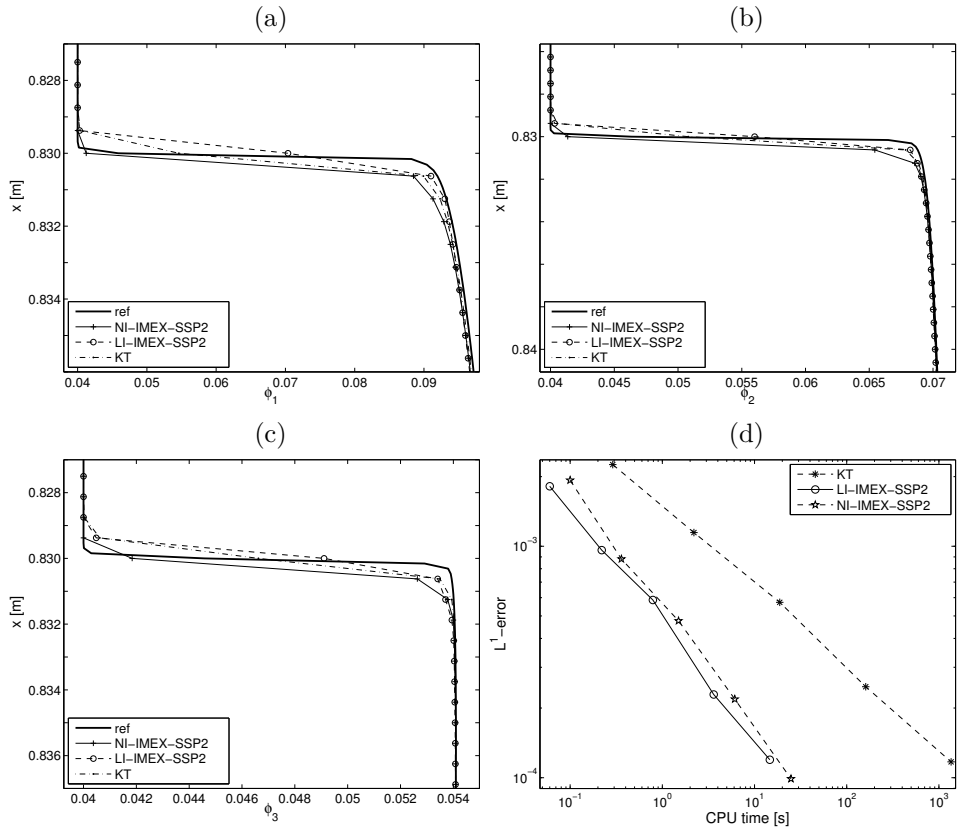

FIG. 4.3. *Example 2 (Model 1, $N = 3$, diffusive term regularized with $\sigma_e(\phi; 10^{-3})$): (a)–(c): enlarged views of the numerical solution near the parabolic-hyperbolic interface ($\phi = \phi_c$), (d): efficiency plot for discretization levels $\Delta x = 1/M$ with $M = 100$, 200, 400, 800 and 1600.*

with $C_{\mathrm{cfl}_2} = 0.6$ are shown in Figure 4.2, we observe that some glitches near the parabolic-hyperbolic interface are still present in the results. In Figure 4.1 (b) we observe that LI-IMEX-SSP2-reg can reduce the approximation error compared with LI-IMEX-SSP2 scheme.

4.3. Examples 2–4: Model 1 with $N = 3$, variation of $\varepsilon_{\min}$. For the tests in Examples 2 to 5, we consider the same data as in Example 1 but apply both schemes LI-IMEX-SSP2 and NI-IMEX-SSP2 to the ε-regularized problems with decreasing values of ε. The linearly implicit scheme keeps solving one linear system per RK stage, whereas the nonlinearly implicit scheme needs several of them and may need the gradual decrease of ε towards $\varepsilon_{\min}$. The reference solution is computed in each example to ε-regularized diffusive term.

In Example 2, we choose a regularized diffusive term with $\varepsilon_{\min} = 10^{-3}$. In the results displayed in Figures 4.3 (a) to (c), which are enlarged views of the results for each component as in Figure 4.1 of Example 1, we observe that the numerical solutions obtained with scheme LI-IMEX-SSP2 do not present overshoots. Moreover, Fig 4.3 (d) shows that it is more efficient than NI-IMEX-SSP2.

Next, in Example 3, we choose the same parameters as in Examples 1 and 2 but regularize the diffusive term by setting $\varepsilon_{\min} = 5 \times 10^{-5}$. This regularization yields

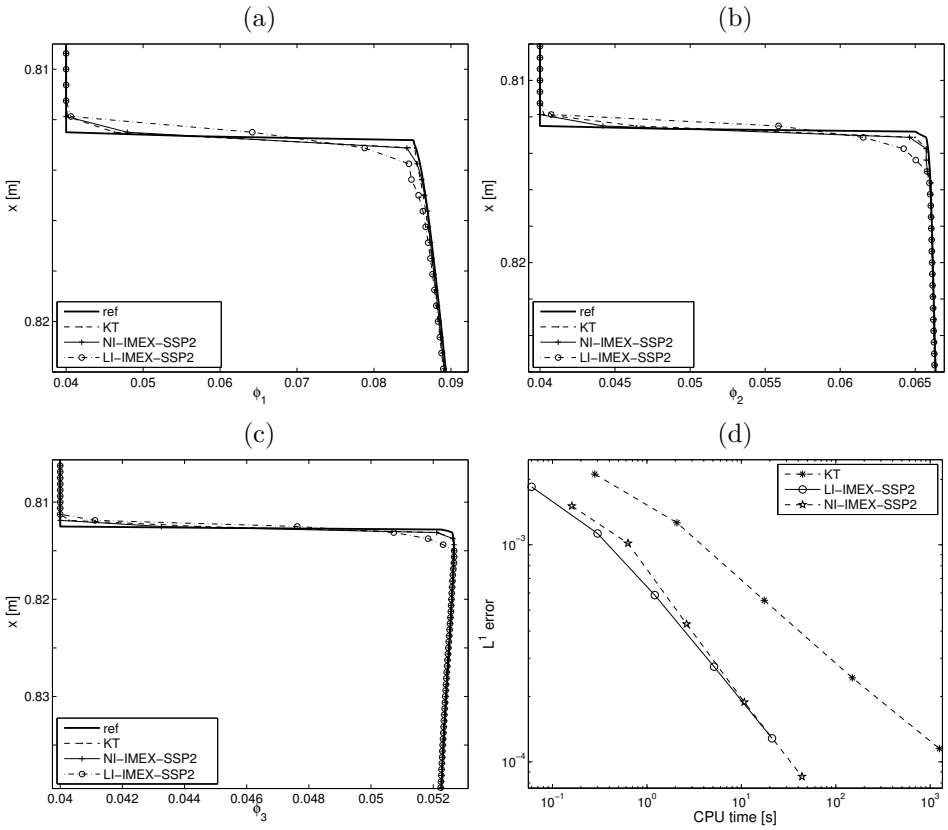

FIG. 4.4. *Example 3 (Model 1, $N = 3$, diffusive term regularized with $\sigma_e(\phi; 5 \times 10^{-5})$): (a)–(c): enlarged views of the numerical solution near the parabolic-hyperbolic interface ($\phi = \phi_c$), (d): efficiency plot for discretization levels $\Delta x = 1/M$ with $M = 100$, 200, 400, 800 and 1600.*

diffusion coefficients that are less smooth than the previous example. Figure 4.4 shows the solutions that are analogous to Figure 4.3 for Example 2. In fact, the solutions displayed in Figs 4.4 (a) to (c) are qualitatively similar and the efficiency curve in Figure 4.4 (d) of scheme LI-IMEX-SSP2 is closer to that of scheme NI-IMEX-SSP2.

Finally, in Example 4 we set $\varepsilon_{\min} = 5 \times 10^{-6}$. We observe in the results displayed in Figure 4.5 (a) to (c) that the numerical solutions obtained with scheme LI-IMEX-SSP2 present some glitches near the parabolic-hyperbolic interface and in Figure 4.5 (d) that the scheme NI-IMEX-SSP2 is slightly more efficient.

4.4. Example 5: Model 1 with $N = 3$, numerical order of accuracy. In this test we check the order of accuracy of the numerical scheme LI-IMEX-SSP2-reg with $\varepsilon_{\min} = 0.1$. We consider the normalized diameters $d_1 = 1.0$, $d_2 = 0.8$, $d_3 = 0.9$ and a smooth initial concentration profile given by $\phi_i(x) = 0.12 \exp(-200(x - 0.5)^2)$ for $i = 1, \ldots, 3$. We compute approximations with $M = 50 \cdot 2^l$, $l = 0, \ldots, 6$, and a fixed time step $\Delta t = 500 \Delta x$, which yields a Courant number of 0.1. Figure 4.6 shows the numerical result for $M = 1600$ for $T = 20\,\mathrm{s}$ (before shock formation, when the solution is still smooth) and for $T = 500\,\mathrm{s}$ (after shock formation).

The approximate L^1-errors $e_M^{\mathrm{tot}}(T)$ defined by (4.1) and their corresponding numerical orders $\theta_M(T)$ given by (4.2) are displayed in Table 4.1 for both $T = 20\,\mathrm{s}$ and

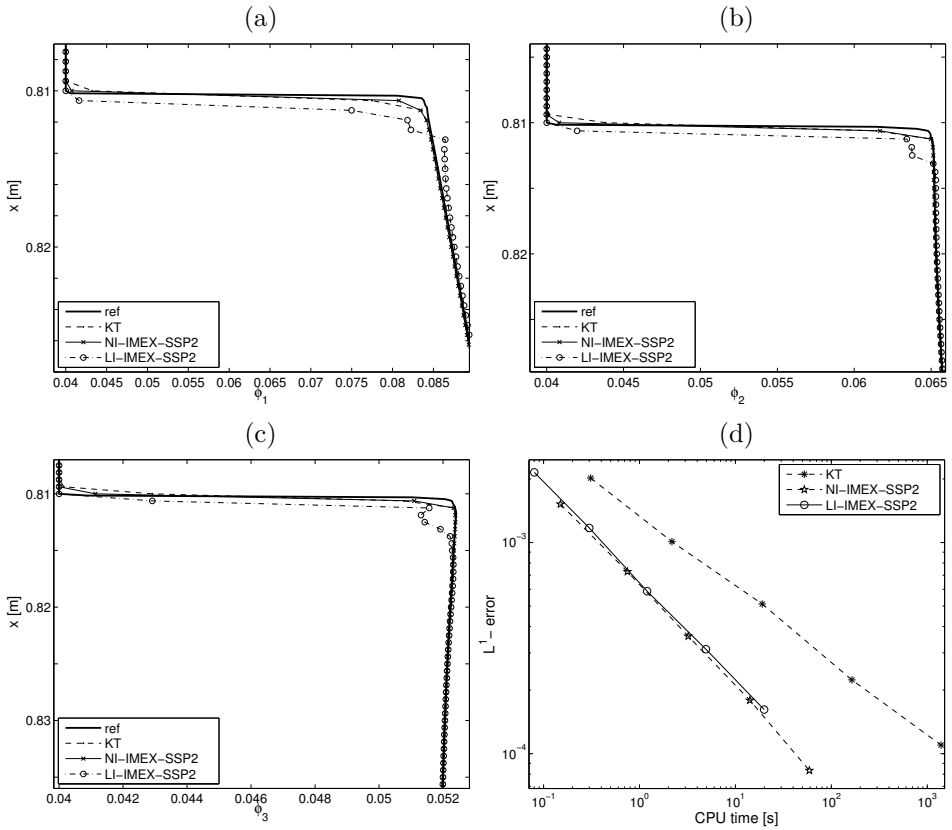

FIG. 4.5. *Example 4 (Model 1, $N = 3$, diffusive term regularized with $\sigma_{\mathrm{e}}(\phi; 5 \times 10^{-6})$): (a)–(c): enlarged views of the numerical solution near the parabolic-hyperbolic interface ($\phi = \phi_{\mathrm{c}}$), (d): efficiency plot for discretization levels $\Delta x = 1/M$ with $M = 100$, 200, 400, 800 and 1600.*

$T = 500\,\mathrm{s}$. The reference solution is computed with $M_{\mathrm{ref}} = 25600$ cells. We select the results for $T = 20\,\mathrm{s}$ to conduct an alternative error analysis (according to Section 4.1). To this end we compute values of $\tilde{e}_M^{\mathrm{tot}}(T)$ according to (4.3), (4.4) (results not shown in Table 4.1) and the corresponding numerical orders of convergence $\hat{\theta}_M(T)$ given by (4.5). The behaviour of both $\theta_M(T)$ and $\hat{\theta}_M(T)$ for increasing values of M confirms that the scheme is second-order accurate for smooth solutions, while the results for $T = 500\,\mathrm{s}$ indicate that accuracy is reduced to first order when shocks are present. Finally, for $T = 20\,\mathrm{s}$ we also calculate the estimate of the total error $\tilde{e}_M^{\mathrm{tot}}(T)$ given by (4.7) for a second-order accurate scheme. Note that for large M, the values of $\tilde{e}_M^{\mathrm{tot}}(T)$ are very close to those of the approximate L^1-errors $e_M^{\mathrm{tot}}(T)$.

4.5. Example 6 (Model 2 with $N = 3$). We consider a circular road of length $K = 5\,\mathrm{mi}$ (periodic boundary conditions (2.12) are used) with $N = 3$ driver classes associated with $v_1^{\max} = 70\,\mathrm{mi/h}$, $v_2^{\max} = 50\,\mathrm{mi/h}$ and $v_3^{\max} = 30\,\mathrm{mi/h}$. We employ the Dick-Greenberg model (2.14) and choose (as in [12, 32]) $C = \mathrm{e}/7 \approx 0.38833$ so that by (2.15), $\phi_{\mathrm{c}} = \exp(-7/\mathrm{e}) \approx 0.076142$. We choose $L_i = L = 0.05\,\mathrm{mi}$ and $\tau_i = \tau = 2\,\mathrm{s} = 0.000\overline{5}\,\mathrm{h}$ for $i = 1, \ldots, N$, such that a particular sufficient condition obtained in [13] for parabolicity on $\mathcal{D}^0_{\phi_{\max}} \backslash \mathcal{D}_{\phi_{\mathrm{c}}}$ is satisfied.

The initial density distribution is given by an isolated platoon of maximum global

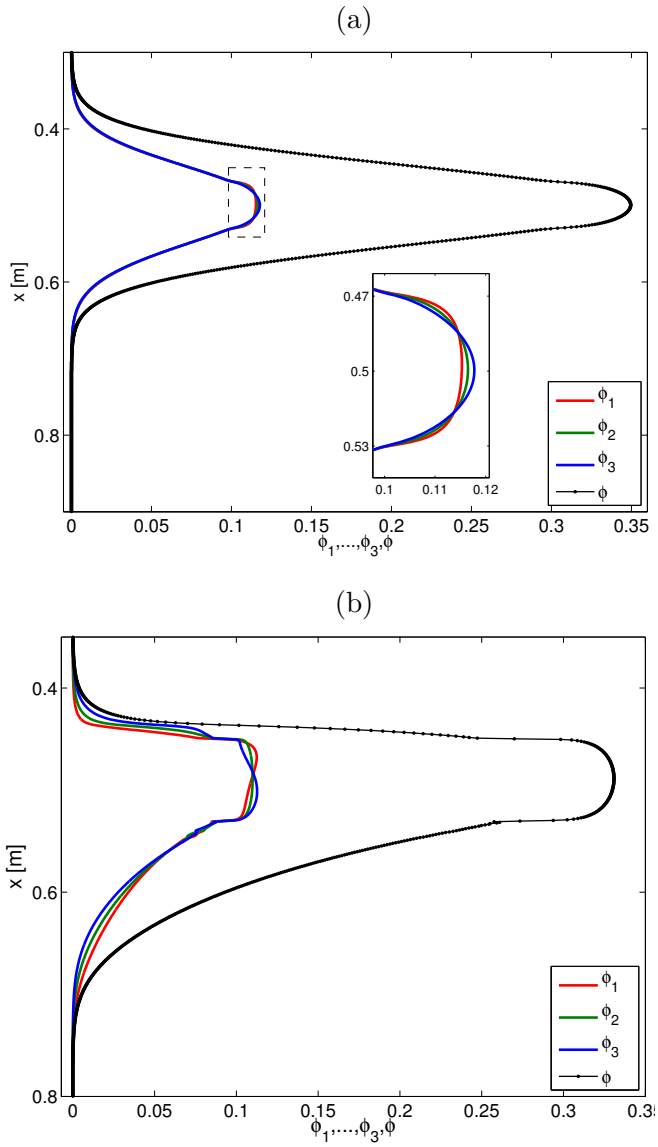

FIG. 4.6. *Example 5 (Model 1, $N = 3$): numerical results obtained by scheme LI-IMEX-SSP2 with $M = 1600$ at simulated time (a) $T = 20\,\mathrm{s}$, (b) $T = 500\,\mathrm{s}$.*

density ρ_0, $\Phi_0(x,0) = p(x-0.3)\rho_0(0.25, 0.4, 0.35)^{\mathrm{T}}$, where $\rho_0 = 0.45$ and

$$p(x) = \begin{cases} 10x & \text{for } 0 < x \le 0.1, \\ 1 & \text{for } 0.1 < x \le 0.9, \end{cases} \qquad \begin{cases} -10(x-1) & \text{for } 0.9 < x \le 1, \\ 0 & \text{otherwise.} \end{cases}$$

The nonlinear systems arising in scheme NI-IMEX-SSP2 are solved by Algorithm 4.1 in [14], where the regularization of the function $V(\phi)$ is given by

$$V(\phi;\varepsilon) = 1 + (V(\phi) - 1)\exp\bigl(-\varepsilon/(\phi - \phi_{\mathrm{c}})^2\bigr), \quad \varepsilon > 0,$$

	$T = 20\,\mathrm{s}$				$T = 500\,\mathrm{s}$	
M	$e_M^{\mathrm{tot}}(T)$	$\theta_M(T)$	$\hat{\theta}_M(T)$	$\tilde{e}_M^{\mathrm{tot}}(T)$	$e_M^{\mathrm{tot}}(T)$	$\theta_M(T)$
50	1.38e-04	0.14	-0.33	8.41e-05	2.27e-03	1.59
100	1.25e-04	1.45	1.48	1.06e-04	7.49e-04	0.95
200	4.58e-05	1.80	1.68	3.80e-05	3.86e-04	1.11
400	1.30e-05	1.88	1.76	1.19e-05	1.78e-04	0.91
800	3.54e-06	1.87	1.87	3.52e-06	9.49e-05	1.05
1600	9.66e-07	2.00	1.98	9.63e-07	4.56e-05	1.01
3200	2.40e-07	2.06	—	2.44e-07	2.26e-05	1.01
6400	5.73e-08	—	—	—	1.12e-05	—

TABLE 4.1

Example 5 (Model 1, $N = 3$): errors and numerical order for scheme NI-IMEX-SSP2 applied to smooth initial conditions for $T = 20\,\mathrm{s}$ (before shock formation) and $T = 500\,\mathrm{s}$ (after shock formation).

where ε varies from $\varepsilon_0 = 10^{-4}$ to $\varepsilon_{\min} = 10^{-6}$ and $\mathrm{tol} = 10^{-7}$.

The reference solution is computed by the KT scheme (without regularization) with $\Delta x = 1/6400$ and $C_{\mathrm{CFL}_2} = 0.25$.

In Figure 4.7 (a) we display the numerical solution obtained by scheme LI-IMEX-SSP2 (without regularization) with $\Delta x = 1/400$ and $C_{\mathrm{CFL}_2} = 0.7$ at simulated time $T = 0.05\,\mathrm{h}$. Enlarged views are shown in Figures 4.7 (b), (c) and (d), where we compare the numerical solution at the same resolution with that produced by scheme NI-IMEX-SSP2 with $C_{\mathrm{CFL}_2} = 0.7$, the KT scheme with $C_{\mathrm{CFL}_1} = 0.25$ and the reference solution. We observe that the approximation obtained by scheme LI-IMEX-SSP2 approximates adequately the reference solution. In Figure 4.8 we display an efficiency plot for a sequence of discretization levels and observe that scheme LI-IMEX-SSP2 is more efficient than NI-IMEX-SSP2.

5. Concluding remarks. The numerical examples presented herein indicate, first of all, that the new linearly implicit IMEX-RK schemes approximate the same solutions as their nonlinearly implicit counterparts (introduced in [14]), and in many cases are more efficient. In the case of the regularized problem with $\epsilon_{\min} = 10^{-3}$ of Example 2, shown in Figure 4.3, the new linearly implicit schemes provide essentially the same results as the classical implicit IMEX at a much lower cost. The decisive advantage of the linearly implicit variant is the ease of implementation. While the numerical examples presented herein have been limited to $N = 3$ for the ease of presentation, this advantage is likely to become more stringent for larger values of N, for example when in the context of the polydisperse sedimentation model (and related applications), a continuous particle size distribution is approximated by N size classes.

Both linearly and nonlinearly implicit IMEX-RK schemes converge to the same solutions as does the KT scheme [28], which provides justfication of their application although a well-posedness theory for (1.1), at least in the strongly degenerate case, is still lacking. However, it turns out that at the same spatial resolution, discontinuities in the solution, especially those associated with the type-change interface, are more accurately resolved by the nonlinearly implicit IMEX-RK schemes. It therefore seems highly desirable to combine the respective advantages of linearly and nonlinearly implicit IMEX-RK schemes by a hybrid scheme that would concentrate the use of the nolinearly implicit variant on regions of presumed irregularities of the solution (such

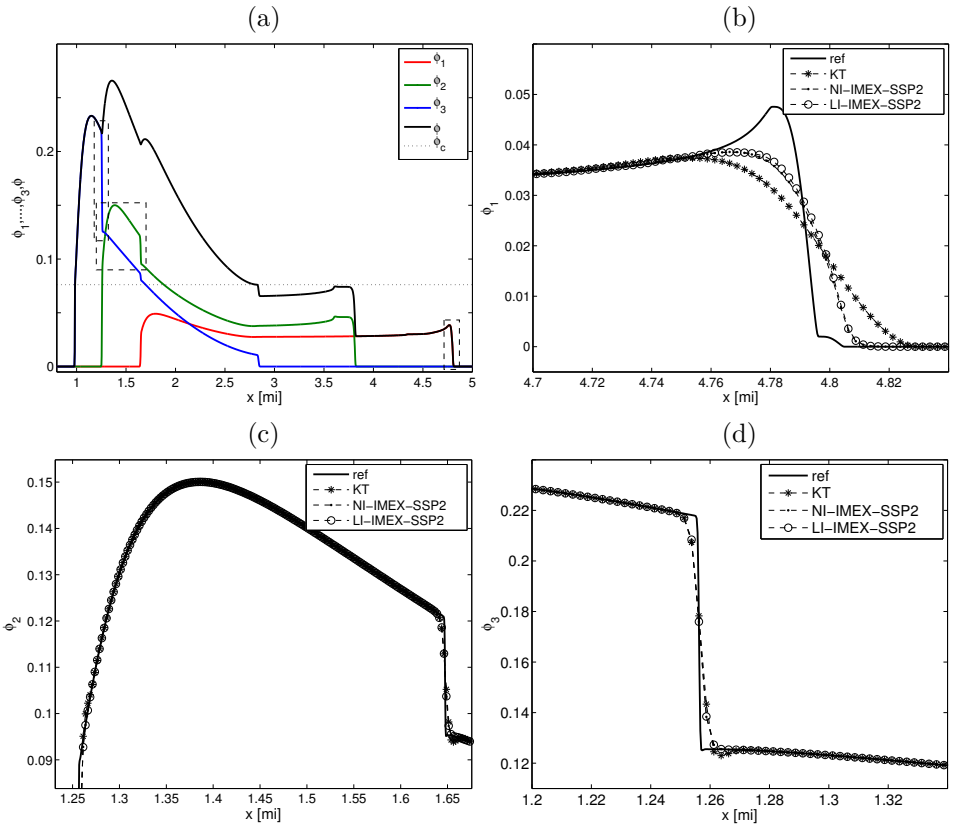

FIG. 4.7. *Example 6 (Model 2, $N = 3$): numerical results at simulated time $T = 0.05\,\mathrm{h}$ (a) obtained by scheme LI-IMEX-SSP2 with $\Delta x = 1/800$, (b)–(d) compared with results by schemes KT and NI-IMEX-SSP2 with $\Delta x = 1/800$ and the reference solution.*

as discontinuities and kinks), which usually form only a small fraction of the computational domain, while in the remaining "smooth" regions the faster linearly implicit variant would be used. In other words, such a scheme would attain an accuracy similar to the nonlinear IMEX-RK one, at a computational cost almost the same as for the linearly implicit version.

The application to diffusively corrected kinematic flow models has been chosen as a test case for IMEX-RK schemes in [14] herein since this class of problems inlcudes systems (1.1) of arbitrary size N, and provides meaningful justification for the assumption of strong degeneracy (2.9). While the linearly and nonlinearly implicit IMEX-RK schemes do not involve the particular algebraic structure of these models, and could therefore also be applied to other models that can be cast in the form (1.1), Theorems 2.1 and 2.2, which do rely on the algebraic structure, are well relevant for the implementation of the WENO-SPEC scheme employed for the discretization of $\partial_x \boldsymbol{f}(\Phi)$ (see [11]). In that context we recall that the WENO reconstruction is based on the computation of smoothness indicators that monitor the presence of irregularities in the solution. We are currently investigating the option to use the same smoothness indicators to design a hybrid scheme of the above-mentioned kind.

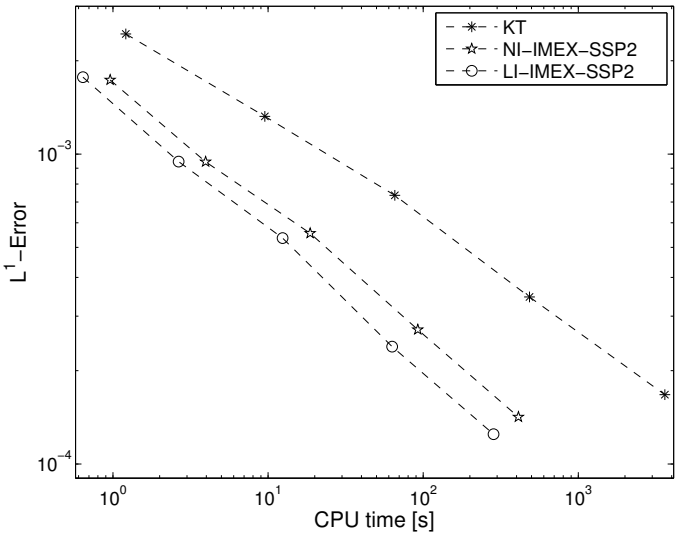

FIG. 4.8. *Example 6 (Model 2, $N = 3$): efficiency plot based on numerical solutions for $\Delta x = 1/M$ with $M = 50$, 100, 200, 400 and 800.*

Acknowledgments. RB is supported by Fondecyt project 1130154; BASAL project CMM, Universidad de Chile and Centro de Investigación en Ingeniería Matemática (CI^{2}MA), Universidad de Concepción; Conicyt project Anillo ACT1118 (ANANUM); Red Doctoral REDOC.CTA, MINEDUC project UCO1202; and CRHIAM, project CONICYT/FONDAP/15130015. PM is partially supported by Spanish MINECO MTM2011-22741. LMV is supported by MECESUP project UCO0713. GR and SB have been partially supported by project PRIN 2009,"Innovative numerical methods of hyperbolic problems with aplications to fluid dynamics, kinetic theory and computational biology", prot.n.2009588FHJ, of the Italian Ministry of Education, University and Research.

Appendix. Assume that the computed approximations $\phi_{j,i}^M(t)$ satisfy

$$\phi_{j,i}^M(t) = \phi_i(x_j,t) + a_i(x_j,t)\Delta x^r + \mathcal{O}(\Delta x^{r+1}), \tag{A.1}$$

where $\Delta x = \mathcal{L}/M$ and $x_j = (j-1/2)\Delta x$, for $r \le 2$ and sufficiently smooth coefficient functions a_j. Then, it can be seen that the quantities defined by (4.3) satisfy

$$\tilde{\phi}_{j,i}^M(t) = \phi_i(x_j,t) + a_i(x_i,t)(\Delta x/2)^r + \mathcal{O}(\Delta x^{r+1}). \tag{A.2}$$

We recall that we calculate an alternative (with respect to (4.1)) total approximate L^1 error from the quantities (4.3) by (4.4), and that the (unknown) exact total error $e_M^{\mathrm{tot},*}(t)$ is given by (4.6). From (A.1), (A.2), and standard quadrature rules we get

$$\hat{e}_M^{\mathrm{tot}}(t) = a(t)(1-2^{-r})\Delta x^r + \mathcal{O}(\Delta x^{r+1}), \quad a(t) = \sum_{i=1}^{N} \int \left|a_i(x,t)\right| \mathrm{d}x,$$

and $e_M^{\mathrm{tot},*}(t) = a(t)\Delta x^r + \mathcal{O}(\Delta x^{r+1})$. We therefore deduce that

$$\lim_{M\to\infty} \left(\hat{e}_M^{\mathrm{tot}}(t)/\hat{e}_{2M}^{\mathrm{tot}}(t)\right) = 2^r \quad \text{and} \quad \lim_{M\to\infty} \left(\hat{e}_M^{\mathrm{tot}}(t)/e_M^{\mathrm{tot},*}(t)\right) = 1-2^{-r},$$

i.e., for the quantity $\hat{\theta}_M(t)$ given by (4.5) we have $\hat{\theta}_M(t) \to r$ as $M \to \infty$, and for large M the exact total error $e_M^{\mathrm{tot},*}(t)$ can be estimated from $\hat{e}_M^{\mathrm{tot}}(t)$ by

$$e_M^{\mathrm{tot},*}(t) \approx \tilde{e}_M^{\mathrm{tot}}(t) := (1 - 2^{-r})^{-1} \hat{e}_M^{\mathrm{tot}}(t), \tag{A.3}$$

which yields (4.7) for $r = 2$.

REFERENCES

[1] A. Abeynaike, A.J. Sederman, Y. Khan, M.L. Johns, J.F. Davidson, and M.R. Mackley, *The experimental measurement and modelling of sedimentation and creaming for glycerol/biodiesel droplet dispersions*, Chem. Eng. Sci., 79 (2012), pp. 125–137.

[2] U. Ascher, S. Ruuth, and J. Spiteri, *Implicit-explicit Runge-Kutta methods for time dependent partial differential equations,* Appl. Numer. Math., 25 (1997), pp. 151–167.

[3] S. Benzoni-Gavage and R.M. Colombo, *An n-populations model for traffic flow*, Eur. J. Appl. Math., 14 (2003), pp. 587–612.

[4] S. Berres, R. Bürger, K.H. Karlsen, and E.M. Tory, *Strongly degenerate parabolic-hyperbolic systems modeling polydisperse sedimentation with compression*, SIAM J. Appl. Math., 64 (2003), pp. 41–80.

[5] S. Boscarino, L. Pareschi, and G. Russo, *Implicit-explicit Runge-Kutta schemes for hyperbolic systems and kinetic equations in the diffusion limit*, SIAM J. Sci. Comput., 35 (2013), pp. A22–A51.

[6] S. Boscarino, P.G. LeFloch, and G. Russo, *High order asymptotic-preserving methods for fully nonlinear relaxation problems*, SIAM J. Sci. Comput., 36 (2014), pp. A377–A395.

[7] S. Boscarino, F. Filbet and G. Russo, *High order semi-implicit schemes for time dependent partial differential equations*, submitted.

[8] S. Boscarino and G. Russo, *On a class of uniformly accurate IMEX Runge-Kutta schemes and applications to hyperbolic systems with relaxation*, SIAM J. Sci. Comput., 31 (2009), pp. 1926–1945.

[9] S. Boscarino and G. Russo, *Flux-explicit IMEX Runge-Kutta schemes for hyperbolic to parabolic relaxation problems*, SIAM J. Numer. Anal., 51 (2013), pp. 163–190.

[10] R. Bürger, R. Donat, P. Mulet, and C.A. Vega, *Hyperbolicity analysis of polydisperse sedimentation models via a secular equation for the flux Jacobian*, SIAM J. Appl. Math., 70 (2010), pp. 2186–2213.

[11] R. Bürger, R. Donat, P. Mulet, and C.A. Vega, *On the implementation of WENO schemes for a class of polydisperse sedimentation models*, J. Comput. Phys., 230 (2011), pp. 2322–2344.

[12] R. Bürger and K.H. Karlsen, *On a diffusively corrected kinematic-wave traffic flow model with changing road surface conditions*, Math. Models Methods Appl. Sci., 13 (2003), pp. 1767–1799.

[13] R. Bürger, P. Mulet, and L.M. Villada, *A diffusively corrected multiclass Lighthill-Whitham-Richards traffic model with anticipation lengths and reaction times*, Adv. Appl. Math. Mech., 5 (2013), pp. 728–758.

[14] R. Bürger, P. Mulet, and L.M. Villada, *Regularized nonlinear solvers for IMEX methods applied to diffusively corrected multi-species kinematic flow models*, SIAM J. Sci. Comput., 35 (2013), pp. B751–B777.

[15] M. Crouzeix, *Une méthode multipas implicite-explicite pour l'approximation des équations d'évolution paraboliques*, Numer. Math., 35 (1980), pp. 257–276.

[16] T.F. Chan, G.H. Golub, and P. Mulet, *A nonlinear primal-dual method for total variation-based image restoration*, SIAM J. Sci. Comput., 20 (1999), pp. 1964–1977.

[17] J.E. Dennis Jr. and R.B. Schnabel, *Numerical Methods for Unconstrained Optimization and Nonlinear Equations*, Classics in Applied Mathematics vol. 16, SIAM, 1996.

[18] A.C. Dick, *Speed/flow relationships within an urban area*, Traffic Engrg. Control, 8 (1996), pp. 393–396.

[19] R. Donat and P. Mulet, *Characteristic-based schemes for multi-class Lighthill-Whitham-Richards traffic models*, J. Sci. Comput., 37 (2008), pp. 233–250.

[20] R. Donat and P. Mulet, *A secular equation for the Jacobian matrix of certain multi-species kinematic flow models*, Numer. Methods Partial Differential Equations, 26 (2010), pp. 159–175.

[21] R. Dorrell, A.J. Hogg, E.J. Sumner, and P.J. Talling, *The structure of the deposit produced by sedimentation of polydisperse suspensions*, J. Geophys. Res., 116 (2011), paper F01024.
[22] H. Greenberg, *An analysis of traffic flow*, Oper. Res., 7 (1959), pp. 79–85.
[23] E. Hairer, S.P. Nørsett, and G. Wanner, *Solving Ordinary Differential Equations. I. Nonstiff problems*, Springer Series in Comput. Mathematics, Vol.8, Springer Verlag, (2nd edition), 1993.
[24] W. Hundsdorfer and J.G. Verwer, Numerical Solution of Time-Dependent Advection-Diffusion-Reaction Equations, Springer, 2003.
[25] K.H. Karlsen and N.H. Risebro, *Convergence of finite difference schemes for viscous and inviscid conservation laws with rough coefficients*, M2AN Math. Modelling Numer. Anal., 35 (2001), pp. 239–269.
[26] K.H. Karlsen and N.H. Risebro, *On the uniqueness and stability of entropy solutions of nonlinear degenerate parabolic equations with rough coefficients*, Discr. Cont. Dyn. Syst., 9 (2003), pp. 1081–1104.
[27] C.A. Kennedy and M.H. Carpenter, *Additive Runge-Kutta schemes for convection-diffusion-reaction equations*, Appl. Numer. Math., 44 (2003), pp. 139–181.
[28] A. Kurganov and E. Tadmor, *New high-resolution central schemes for nonlinear conservation laws and convection-diffusion equations*, J. Comput. Phys., 160 (2000), pp. 241–282.
[29] M.J. Lighthill and G.B. Whitham, *On kinematic waves: II. A theory of traffic flow on long crowded roads*, Proc. Royal Soc. A, 229 (1955), pp. 317–345.
[30] M.J. Lockett and K.S. Bassoon, *Sedimentation of binary particle mixtures*, Powder Technol., 24 (1979), pp. 1–7.
[31] J.H. Masliyah, *Hindered settling in a multiple-species particle system*, Chem. Engrg. Sci., 34 (1979), pp. 1166–1168.
[32] P. Nelson, *Synchronized traffic flow from a modified Lighthill-Whitham model*, Phys. Rev. E, 61 (2000), pp. R6052–R6055.
[33] J.M. Ortega and W.C. Rheinboldt, *Iterative Solution of Nonlinear Equations in Several Variables.* Classics in Applied Mathematics. SIAM, 1987.
[34] L. Pareschi and G. Russo, *Implicit-Explicit Runge-Kutta schemes and applications to hyperbolic systems with relaxation,* J. Sci. Comput., 25 (2005), pp. 129-155.
[35] P.I. Richards, *Shock waves on the highway*, Oper. Res., 4 (1956), pp. 42–51.
[36] J.F. Richardson and W.N. Zaki, *Sedimentation and fluidization: Part I*, Trans. Instn. Chem. Engrs. (London), 32 (1954), pp. 35–53.
[37] F. Rosso and G. Sona, *Gravity-driven separation of oil-water dispersions*, Adv. Math. Sci. Appl., 11 (2001), pp. 127–151.
[38] E. Rouvre and G. Gagneux, *Solution forte entropique de lois scalaires hyperboliques-paraboliques dégénérées*, C. R. Acad. Sci. Paris Sér. I, 329 (1999), pp. 599–602.
[39] C.-W. Shu, *Essentially non-oscillatory and weighted essentially non-oscillatory schemes for hyperbolic conservation laws.* In: B. Cockburn, C. Johnson, C.-W. Shu, and E. Tadmor, *Advanced Numerical Approximation of Nonlinear Hyperbolic Equations* (A. Quarteroni, Ed.), Lecture Notes in Mathematics vol. 1697, Springer-Verlag, Berlin (1998), pp. 325–432.
[40] C.-W. Shu, *High order weighted essentially nonoscillatory schemes for convection dominated problems*, SIAM Rev., 51 (2009), pp. 82–126.
[41] C.-W. Shu and S. Osher, *Efficient implementation of essentially non-oscillatory shock-capturing schemes, II*, J. Comput. Phys., 83 (1989), pp. 32–78.
[42] G.C.K. Wong and S.C. Wong, *A multi-class traffic flow model—an extension of LWR model with heterogeneous drivers*, Transp. Res. A, 36 (2002), pp. 827–841.
[43] M. Zhang, C.-W. Shu, G.C.K. Wong, and S.C. Wong, *A weighted essentially non-oscillatory numerical scheme for a multi-class Lighthill-Whitham-Richards traffic flow model*, J. Comput. Phys., 191 (2003), pp. 639–659.
[44] X. Zhong, *Additive semi-implicit Runge-Kutta methods for computing high-speed nonequilibrium reactive flows*, J. Comput. Phys., 128 (1996), pp. 19–31.